The Journal of Chemical Physics

Thermodynamic, transport, and structural properties of hydrophobic deep eutectic solvents composed of tetraalkylammonium chloride and decanoic acid

Cite as: J. Chem. Phys. **154**, 144502 (2021); https://doi.org/10.1063/5.0047369
Submitted: 12 February 2021 • Accepted: 25 March 2021 • Published Online: 09 April 2021

Hirad S. Salehi, Alper T. Celebi, Thijs J. H. Vlugt, et al.

AIP Publishing

The Journal of Chemical Physics ARTICLE scitation.org/journal/jcp

Thermodynamic, transport, and structural properties of hydrophobic deep eutectic solvents composed of tetraalkylammonium chloride and decanoic acid

Cite as: J. Chem. Phys. 154, 144502 (2021); doi: 10.1063/5.0047369
Submitted: 12 February 2021 • Accepted: 25 March 2021 •
Published Online: 9 April 2021

Hirad S. Salehi, Alper T. Celebi, Thijs J. H. Vlugt, and Othonas A. Moultos[a)]

AFFILIATIONS

Engineering Thermodynamics, Process and Energy Department, Faculty of Mechanical, Maritime and Materials Engineering, Delft University of Technology, Leeghwaterstraat 39, 2628CB Delft, The Netherlands

Note: This paper is part of the JCP Special Topic on Chemical Physics of Deep Eutectic Solvents.
[a)]**Author to whom correspondence should be addressed:** O.Moultos@tudelft.nl

ABSTRACT

With the emergence of hydrophobic deep eutectic solvents (DESs), the scope of applications of DESs has been expanded to include situations in which miscibility with water is undesirable. Whereas most studies have focused on the applications of hydrophobic DESs from a practical standpoint, few theoretical works exist that investigate the structural and thermodynamic properties at the nanoscale. In this study, Molecular Dynamics (MD) simulations have been performed to model DESs composed of tetraalkylammonium chloride hydrogen bond acceptor and decanoic acid hydrogen bond donor (HBD) at a molar ratio of 1:2, with three different cation chain lengths (4, 7, and 8). After fine-tuning force field parameters, densities, viscosities, self-diffusivities, and ionic conductivities of the DESs were computed over a wide temperature range. The liquid structure was examined using radial distribution functions (RDFs) and hydrogen bond analysis. The MD simulations reproduced the experimental density and viscosity data from the literature reasonably well and were used to predict diffusivities and ionic conductivities, for which experimental data are scarce or unavailable. It was found that although an increase in the cation chain length considerably affected the density and transport properties of the DESs (i.e., yielding smaller densities and slower dynamics), no significant influence was observed on the RDFs and the hydrogen bonds. The self-diffusivities showed the following order for the mobility of the various components: HBD > anion > cation. Strong hydrogen bonds between the hydroxyl and carbonyl groups of decanoic acid and between the hydroxyl group of decanoic acid and chloride were observed to dominate the intermolecular interactions.

I. INTRODUCTION

Deep eutectic solvents (DESs) are a class of designer solvents, first introduced by Abbott *et al.*[1] in 2003. In that study, a mixture of choline chloride and urea was shown to have a melting point significantly lower than those of the individual components, forming a liquid phase at room temperature. Ever since, numerous DESs have been reported in the literature, which share properties such as easy preparation, low melting points, tunability, negligible vapor pressure, non-toxicity, biodegradability, and good solvation properties with respect to different solutes.[2–8] Due to these properties, DESs are often stated to be potentially superior solvents and reaction media, compared to conventional solvents used in industry.[2,9] Nevertheless, it is important to note that the properties of DESs strongly depend on the starting compounds and the composition, and thus, such general statements should be avoided.[6,10]

Several classes of DESs have been reported in the literature based on the chemical nature of the precursors used to synthesize the DES. Smith *et al.*[4] categorized DESs into mixtures composed of (I) salts and metal halides, (II) salts and metal halide hydrates, (III) organic salts and hydrogen bond donors (HBDs) (the most common DESs), and (IV) metal halides and hydrogen bond donors.

DESs based on natural and charge-neutral compounds have also been investigated in the literature.[7,11] Recently, a new class of DESs based on phenolic hydrogen bond donating groups was introduced by Abranches *et al.*[12]

Although DESs are often identified by a large melting point depression of the mixture and an extensive hydrogen bonding network, the precise definition of a DES is debated.[10,13,14] For instance, it has been suggested that a considerable difference between the eutectic point of the mixture and the ideal solution eutectic point (and not the melting points of the individual components) is necessary for the definition of a DES.[10,13] The necessity of hydrogen bonds for the formation of DESs has also been questioned.[10,13] Based on these alternative definitions, many of the reported DESs are classified as simple eutectic mixtures rather than "deep" eutectic solvents.[10] Therefore, the solid–liquid phase equilibrium of the mixture must be well-characterized before the solvent is labeled "DES."

For many years, the DESs reported in the literature were of hydrophilic nature until van Osch *et al.*[15] introduced a new hydrophobic class of DESs for the first time in 2015. These DESs are often a mixture of hydrogen bond donors (HBDs) and hydrogen bond acceptors (HBAs). The HBA and HBD components are charge-neutral or charged (salts composed of cations and anions) hydrophobic compounds with hydrophobic functional groups (e.g., long alkyl chains). Hydrophobic DESs have attracted much attention as water-immiscible solvents with many potential applications ranging from carbon capture to water purification and extraction of metabolites from plants.[6,14] DESs based on tetraalkylammonium halides and fatty acids (e.g., decanoic acid), for instance, have been considered for a large number of applications, such as CO_2 capture,[16–18] extraction of fatty acids,[15] antibiotics,[19] sugar-derived molecules,[20,21] and metal ions[22–24] from aqueous solutions, and extraction of pigments from different beverages.[25] It has been shown by van Osch *et al.*[15] that the degree of hydrophobicity (based on the cation chain length) of these DESs determines the extent to which the DES leaches into the water phase and affects the extraction process from aqueous solutions. For a more detailed discussion on the various applications of hydrophobic DESs, the reader is referred to the review article by van Osch *et al.*[6]

Most of the studies on hydrophobic DESs have concentrated on the application of these solvents rather than fundamental investigation of intermolecular interactions and the effects of these interactions on the macroscopic properties of DESs.[14] Therefore, systematic knowledge on the liquid structure and the dominant intermolecular interactions between various components of these mixtures is largely lacking. Limited literature is available on theoretical modeling of hydrophobic DESs, where mainly COSMO-based[26–29] and PC-SAFT equations of state modeling[16,17,20,21] techniques are used. Despite the widespread use of Molecular Dynamics (MD) simulations for hydrophilic DESs,[30–42] very few publications are available for hydrophobic DESs.[43,44] In the studies by Verma *et al.*[43] and Paul *et al.*,[44] MD simulations were used to model the stability and thermodynamic properties of hydrophobic DESs based on DL-menthol and tetrabutylammonium chloride HBAs in the presence of water. However, the authors mainly reported aqueous solution properties rather than properties of pure DESs (except for a few density data). Furthermore, the force field validation for the DESs was performed solely based on experimental densities, which may decrease the suitability of the developed force fields for the calculation of other thermo-physical properties, such as the viscosity, and limit the transferability of the force field parameters.

In this work, MD simulations have been used for the first time to study the liquid structure and thermodynamic and transport properties of hydrophobic DESs based on tetraalkylammonium chloride (TRAC) salts as the HBA compound and decanoic acid (a long-chain fatty acid) as the HBD compound in a HBA:HBD molar ratio of 1:2. To examine the influence of the alkyl chain length of the cation (i.e., number of alkyl chain carbons) and thus the hydrophobicity of the DESs on the liquid structure and physico-chemical properties, various cation chain lengths were used in the simulations: 4 (butyl), 7 (heptyl), and 8 (octyl). The respective DESs are designated as TBAC-dec, THAC-dec, and TOAC-dec. To the best of our knowledge, no other molecular simulation studies exist that systematically investigate the thermo-physical and structural properties of TRAC-based hydrophobic DESs and the effect of cation chain length on those properties. These DESs were considered here due to their many potential applications, particularly in liquid–liquid extraction of solutes,[15,22,24,25] as previously discussed. In the case of extraction from aqueous solutions, the miscibility of hydrophobic DESs with water must be quantified. In this work, the focus has been on the properties of pure DESs, and therefore, the miscibility with water is not discussed. However, well-established methods, such as particle insertions and thermodynamic integration, can in principle be used to compute the solubility of water in DESs.[41,45,46] It is important to note that TRAC + fatty acid DESs exhibit significant negative deviations from ideality, which increase with the cation chain length.[47] Therefore, a eutectic point temperature lower than that of the ideal solution eutectic point is observed for these mixtures, rendering them as "deep" eutectic mixtures.[10] Although the prediction of melting point and thus solid/liquid phase equilibrium of ionic liquids (ILs) and DESs from molecular simulations can be of great practical interest, these calculations are often challenging for such complex molecules and may not yield accurate results.[48]

This manuscript is organized as follows: In Sec. II, the computational methods used in this study are described. This includes the force field parameters of the DESs, simulation details, and the methods used to compute thermodynamic, transport, and structural properties. Subsequently, force field validation and simulation results are discussed and compared with available data in the literature. In the end, conclusions are provided regarding the MD simulation of TRAC-dec DESs.

II. COMPUTATIONAL DETAILS

The non-polarizable all-atom general AMBER force field (GAFF)[49] was used for modeling all DESs. Non-bonded terms, consisting of Lennard-Jones (LJ) and electrostatic energies, as well as bonded terms (bond-stretching, bond-bending, and torsion) were used to model the intermolecular and intramolecular interactions. The LJ parameters by Fox and Kollman[50] were used for chloride anions. The electrostatic potential was computed for the optimized geometry of each isolated individual molecule or ion at the

HF/6-31G* level of theory, and the partial atomic charges were obtained using the restrained electrostatic potential (RESP) method.[51] Geometry optimization and charge calculations were performed using the Gaussian 09 Rev.B.01 software[52] and the R.E.D-III.52 tools.[53] It has been shown that commonly used classical force fields, e.g., GAFF, often overestimate intermolecular interactions of ILs and DESs, which results in slower dynamics, i.e., smaller diffusivities and larger viscosities, compared to experimental observations.[32,54,55] To obtain a better agreement of the simulation results with experimental data, strategies based on scaling of ionic (partial) charges[30–34,41,54,56,57] and/or LJ interactions[58,59] have therefore been proposed in the literature as computationally efficient solutions. Here, a combination of ionic charge scaling factors (f_q) in the range of 0.6–1.0 and LJ well-depth (ε) scaling factors (f_ε) in the range of 0.9–1.0 was examined. The ionic charge scaling factors were only applied to the (partial) charges of cations and anions. The scaling of the σ parameter of LJ potential was not considered due to the drastic adverse effect on the density, observed in preliminary test simulations. Following the approach by Jamali *et al.*[60] for carbohydrates, the LJ scaling factors were used for all atoms in the DES mixtures. This is in contrast to the approach by Chaumont *et al.*,[59] where only LJ interactions of specific atoms (hydroxyl hydrogen and oxygen) were modified for choline chloride ethylene glycol and choline chloride glycerol DESs. The latter approach was not employed in this work, as it may introduce extra complication to the optimization procedure.[60] Molecular structures and optimal force field parameters for all the DES components are listed in the supplementary material. The 1–4 intramolecular electrostatic and LJ interactions were scaled by 0.833 and 0.5, respectively, in accordance with the AMBER force field.[61] The Particle–Particle Particle–Mesh (PPPM) method[45] with a relative error of 10^{-6} was used to computed the long-range electrostatic energies. A cutoff radius of 12 Å was used for both the short-range LJ and electrostatic energies. Analytic tail corrections[46] were used to account for the contributions to LJ energies and pressure beyond the cutoff radius. The Lorentz–Berthelot mixing rules were applied to obtain the LJ interactions between non-identical atom types. The Nosé–Hoover thermostat and barostat[45] were used to impose the temperature and pressure, respectively. The Verlet algorithm[45,62] was used to integrate the equations of motion with a time step of 1 fs. Initial low-density configurations were constructed using the PACKMOL package,[63] and the simulations were carried out with the LAMMPS software[64] (version 16 March 2018). The VMD[65] visualization software was used to view snapshots of the system and perform hydrogen bond analysis (with the HBonds plugin).

In all simulations, the energy of the system was initially minimized using the conjugate-gradient method to remove atomic overlaps. After equilibration of the system over 40 ns, the average density of the DESs was computed at 1 atm and various temperatures in the isobaric–isothermal (*NPT*) ensemble over 20 ns. It is important to note that such long equilibration times were necessary, particularly at lower temperatures, for a complete convergence of the density and total energy. This is possibly due to the high viscosity of the DESs and entanglement of the long alkyl chains. After performing the *NPT* simulations, transport and structural properties were computed at various temperatures in the canonical (*NVT*) ensemble, where the simulation box size was set according to the average densities obtained from the *NPT* simulations. The *NVT* simulations consisted of 10 ns equilibration and 440–650 ns (depending on the DES and the temperature) production runs, respectively. For each data point, five independent simulations were run, over which averages and standard deviations were calculated. For enhanced equilibration and circumvention of local energy minima, annealing of the system was performed at elevated temperatures (600 and 400 K) for 8 ns before both the *NPT* and *NVT* equilibration runs. All simulations consisted of 50 HBA (50 tetraalkylammonium cations and 50 chloride anions) and 100 decanoic acid HBD molecules, corresponding to a HBA:HBD molar ratio of 1:2. The OCTP plugin[66] in LAMMPS was used for computation of transport properties and finite size-corrected radial distribution functions (RDFs).[67,68] The computations by the OCTP package are performed on-the-fly, and thus, atomic trajectories were not printed from the simulations for post-processing and obtaining the properties.

The OCTP package computes transport properties with the order-n algorithm[45,69] using Einstein relations. The shear viscosity of the system was obtained from the production runs using[46]

$$\eta = \lim_{t\to\infty} \frac{1}{2t}\frac{V}{k_B T}\left\langle \left(\int_0^t P_{\alpha\beta}(t')\mathrm{d}t' \right)^2 \right\rangle, \tag{1}$$

where $\langle\cdots\rangle$ denotes an ensemble average, $P_{\alpha\beta}$ (α, β = x, y, z and $\alpha \neq \beta$) is any of the off-diagonal components of the pressure tensor for an isotropic system, V is the volume of the simulation box, t is the time, T is the temperature, and k_B is the Boltzmann constant.

The self-diffusion coefficient of species i, $D^{\mathrm{MD}}_{\mathrm{self},i}$, in the DES mixture was computed from the last 100–200 ns of the production runs according to[46,70]

$$D^{\mathrm{MD}}_{\mathrm{self},i} = \lim_{t\to\infty} \frac{1}{6N_i t}\left\langle \sum_j^{N_i} |\mathbf{r}_{ji}(t) - \mathbf{r}_{ji}(0)|^2 \right\rangle, \tag{2}$$

where $\mathbf{r}_{ji}$ is the position vector of molecule j of species i and N_i is the total number of molecules of species i. Unlike the shear viscosity, self-diffusion coefficients are known to significantly depend on the system size.[70–72] The Yeh–Hummer correction was used to obtain the diffusion coefficient of each species i in the thermodynamic limit, $D^{\infty}_{\mathrm{self},i}$, as[70,73,74]

$$D^{\infty}_{\mathrm{self},i} = D^{\mathrm{MD}}_{\mathrm{self},i} + \frac{k_B T \xi}{6\pi\eta L}, \tag{3}$$

where L is the simulation box length, η is the shear viscosity of the system computed from MD simulations [from Eq. (1)], and ξ is a constant with a value of 2.837298 for a periodic lattice.

The ionic conductivity of each DES was estimated according to the Nernst–Einstein equation as[75]

$$\kappa = \frac{e^2}{k_B T V}\sum_i N_i q_i^2 D^{\infty}_{\mathrm{self},i}, \tag{4}$$

where the summation runs over all molecule/ion types i, q_i, and N_i are the net charge and number of molecules of type i, respectively, V is the volume of the simulation box, and e is the elementary

charge. Since only the diffusion coefficients [and indirectly the viscosities, via Eq. (3)] from the simulations are used in Eq. (4), no additional computations are required to obtain the ionic conductivities using the Nernst–Einstein relation. The Ionic conductivity can also be computed using the Green–Kubo or Einstein relations, which take into account the cross correlation of charge fluxes/displacements.[75–77] To be able to use the Green–Kubo or Einstein relations, atomic trajectories would be required at a sufficient sampling frequency, and extensive subsequent post-processing must be performed. Therefore, for simplicity, the Nernst–Einstein relation was used in this work. Furthermore, Celebi *et al.*[33] have shown that the Nernst–Einstein equation yields a reasonable accuracy for the ionic conductivity of the aqueous solution of choline chloride urea DESs in a wide range of water mass fractions and temperatures.

The liquid structure of the DES mixtures was analyzed using the finite size-corrected RDFs for various atom pairs.[67,68] The first solvation shell coordination numbers were computed by integrating the RDFs up to the first minimum. The number of various types of hydrogen bonds was computed from snapshots of atomic trajectories over the last 100–150 ns (depending on the DES) of the production runs. The criteria for the detection of hydrogen bonds were set to a donor–hydrogen–acceptor angle of 30° and a (heavy-to-heavy atom) cutoff distance of 3.5 Å.[30,33,78–80]

III. RESULTS AND DISCUSSION

A. Thermodynamic and transport properties

1. Force field validation

Force field fine-tuning was performed for TBAC-dec using different charge and LJ scaling factors, and the obtained parameters were evaluated for the other DESs. The force field development was hindered by inconsistencies observed between the experimental data reported in the literature. For instance, van Osch *et al.*[15] reported the viscosities of TBAC-dec, THAC-dec, and TOAC-dec at 298 K as 265, 173, and 473 cP, respectively, showing no clear trend with respect to the cation chain length. The authors noted water contents of 8140, 7740, and 4640 ppm for TBAC-dec, THAC-dec, and TOAC-dec, respectively. The amount of water content has been shown to have a significant effect on the viscosity of TBAC-dec[24] as well as other (hydrophilic) DESs.[81–83] Assuming that the reported values are on a mass fraction basis, the mole fraction-based water content of THAC-dec (10.2%) in the study by van Osch *et al.*[15] was larger than that of TBAC-dec (8.6%), which may have resulted in the lower viscosity of THAC-dec. As an another example, the experimental viscosity of TBAC-dec at 298 K is reported to be 265,[15] 429,[24] and 489 cP[84] in different studies. This disparity between the viscosity values may also be attributed to variations in the water content of the DESs, or may be due to inaccuracy of the experimental measurements. Such inconsistencies have also been reported for hydrophilic DESs.[41] In this work, the simulation results were compared with the experimental data by van Osch *et al.*,[15] except for the viscosity of THAC-dec.

The density and viscosity of TBAC-dec based on different charge and LJ scaling factors are presented in Fig. 1. Due to slow dynamics of the DESs, the calculation of transport properties, including the viscosity, was restricted to relatively elevated temperatures ($T \geq 323$ K). The experimental viscosity data of van Osch *et al.*[15] show an Arrhenius-type temperature dependence (with a correlation coefficient of $R^2 = 0.9994$) and were therefore extrapolated to higher temperatures for the purpose of comparison with the MD calculations. It can be observed in Fig. 1 that the density and viscosity of TBAC-dec decrease by reducing the LJ and ionic charge scaling factors (farther from 1) due to the weakening of intermolecular interactions. As shown in Fig. 1, the combination of $f_q = 0.6$ and $f_\varepsilon = 1.0$ (no scaling) yields a reasonable agreement of the simulation results with the experimental data with average relative deviations of 1.72% and 15% for density and viscosity, respectively. It should be noted that $f_q = 0.6$ is smaller than the ionic charge scaling factors commonly used in simulations of DESs and ILs (0.7–0.9),[30–34,36,39,41,57,85–87] although occasionally the use of

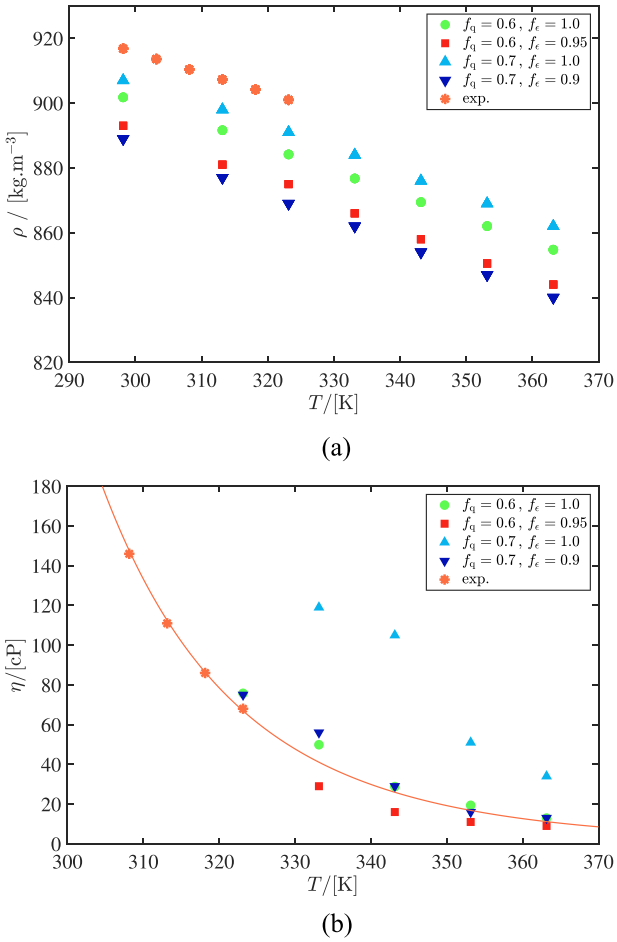

FIG. 1. (a) Density and (b) viscosity of TBAC-dec as a function of temperature with various ionic charge scaling (f_q) and LJ scaling (f_ε) factors, compared with experimental data by van Osch *et al.*[15] The solid curve in (b) depicts the Arrhenius fit to the experimental data.

scaling factors in the range of 0.6–0.7 has also been reported.[55,88] As far as hydrophobic DESs are concerned, Paul *et al.*[44] reported no use of charge scaling for TBAC-octanoic acid DES (nor for the more hydrophilic TBAC-acetic acid DES). However, the authors only validated the force field parameters based on density, which, in contrast to viscosity, is not significantly influenced by this scaling factor, as can be clearly seen in Fig. 1. Details on the use/non-use of charge scaling are not mentioned in the MD studies by Shah *et al.*[89] and Verma *et al.*[43]

It has been suggested that for ILs the ionic charge scaling factor is correlated with the dielectric constant (as $1/\sqrt{\varepsilon_{el}}$) and refractive index (as $1/n_D$).[90,91] Although such correlations are not established for DESs, the relatively small values of f_q for TBAC-dec in this work may suggest large polarizability. To the best of our knowledge, dielectric constant and refractive index data are not available for TBAC-dec to corroborate this. The Kamlet–Taft dipolarity/polarizability parameter, π^*, of TBAC-dec has been reported as 0.73,[92] along with other TRAC-carboxylic acids having π^* values ranging from 0.69 to 1.06.[92,93] These values are typically lower than those of choline chloride-based DESs (1.00–1.23),[94] for which charge scaling values of 0.8 and 0.9 are mostly used in simulation studies.[30,31,33,39,57] This suggests a lower dipolarity/polarizability of TRAC-carboxylic acid (including TBAC-dec) DESs. Chaumont *et al.*[59] have suggested that the effectiveness of the charge scaling approach is, however, not due to the accounting for polarizability and charge transfer processes, but it is rather caused by the overestimation of charges from the commonly used charge derivation techniques. Schröder[86] has also argued that the scaled-charge models do not represent the average polarizability, although the scaling factors may be seen as useful additional force field parameters that improve the accuracy of computation of transport properties.

As shown in Fig. 1(b), using a larger f_q (i.e., 0.7 instead of 0.6) for TBAC-dec results in significantly slower dynamics of the system and consequently larger viscosities that are far from experimental data. This issue may be overcome by using $f_\varepsilon < 1.0$. A combination of $f_q = 0.7$ and $f_\varepsilon = 0.9$ results in similar viscosities compared to $f_q = 0.6$ and $f_\varepsilon = 1.0$ [Fig. 1(b)]. Nonetheless, due to the adverse effect of LJ scaling on density [Fig. 1(a)], $f_q = 0.6$ and $f_\varepsilon = 1.0$ were chosen as the optimal scaling factors. Therefore, the values $f_q = 0.6$ and $f_\varepsilon = 1.0$ were used for all DESs in all production runs of this work. A typical snapshot from the simulation of TBAC-dec with the optimal force field parameters is shown in Fig. 2. As mentioned in Sec. II, the LJ parameters by Fox and Kollman[50] ($\varepsilon = 0.265$ kcal mol^{-1} and $\sigma = 3.471$ Å) were used for chloride anions, as the standard GAFF parameters ($\varepsilon = 0.100$ kcal mol^{-1} and $\sigma = 4.401$ Å) were observed to considerably underestimate the densities of all DESs (for all f_q values). For instance, the density of TBAC-dec (with $f_q = 0.6$) using the standard GAFF parameters for chloride was computed as 867 kg m^{-3} at 298 K. With the chloride LJ parameters by Fox and Kollman,[50] however, a density of 902 kg m^{-3} was computed, which is in a closer agreement (by 3.8%) with the experimental measurement (917 kg m^{-3}).[15] It is interesting that the standard GAFF LJ parameters for chloride have been shown to accurately reproduce experimental densities of choline chloride-based hydrophilic DESs,[30,31,39] in contrast to the DESs in the present study. This clearly indicates the crucial role of chloride anions in molecular packing within TRAC-dec hydrophobic DESs and, hence, the necessity for LJ parameters with larger well-depths and less repulsive cores.

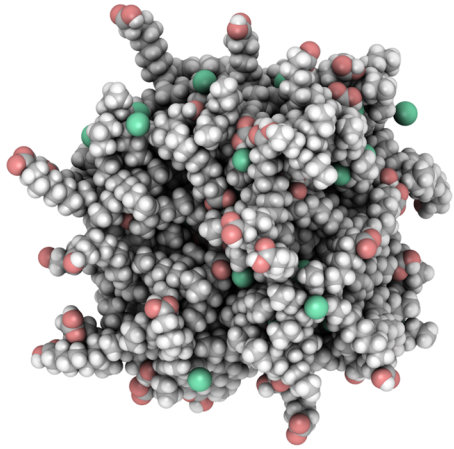

FIG. 2. A typical snapshot from MD simulation of TBAC-dec at 343.15 K and 1 atm, generated by iRASPA.[95]

2. Densities

The computed densities of all DESs (with the optimal force field parameters) are presented as a function of temperature in Fig. 3(a) and as a function of cation alkyl chain length at 323.15 K in Fig. 3(b). The computed density values for all DESs are also listed in Table S12 of the supplementary material. It can be observed in Fig. 3 that the MD results are in close agreement with the experimental data by van Osch *et al.*[15] for all DESs. The average relative deviations of the computed densities from the experimental data are 1.72%, 0.65%, and 0.79% for TBAC-dec, THAC-dec, and TOAC-dec, respectively. Furthermore, the linear reduction of density with an increase in temperature is well captured from MD simulations. From the slope of the computed densities as a function of temperature, the volumetric thermal expansion coefficients were calculated as ~8.3×10^{-4} K^{-1} for all DESs. This is in agreement with the values computed from the experimental densities by van Osch *et al.*,[15] i.e., ~7.0×10^{-4} K^{-1} for TBAC-dec and ~7.3×10^{-4} K^{-1} for THAC-dec and TOAC-dec. As shown in Fig. 3(b), the computed density decreases as the cation chain length is increased from 4 to 8, which is consistent with the experimental data, although the slopes of this decrease are somewhat different. The reduction in density with an increase in the cation chain length is also reported for ILs[96–99] and other DESs[100–103] in the literature and is the opposite of the trend found for alkanes.[104] This effect may be attributed to the steric hindrance of the cation chains, which hampers the packing of molecules.[96,98,101]

3. Viscosities

The viscosities of TBAC-dec and TOAC-dec as a function of temperature are presented and compared with experimental data in Fig. 4. As expected, an increase in temperature results in enhanced molecular motions and thus lower viscosities of both DESs. The computed values for the viscosity of THAC-dec from

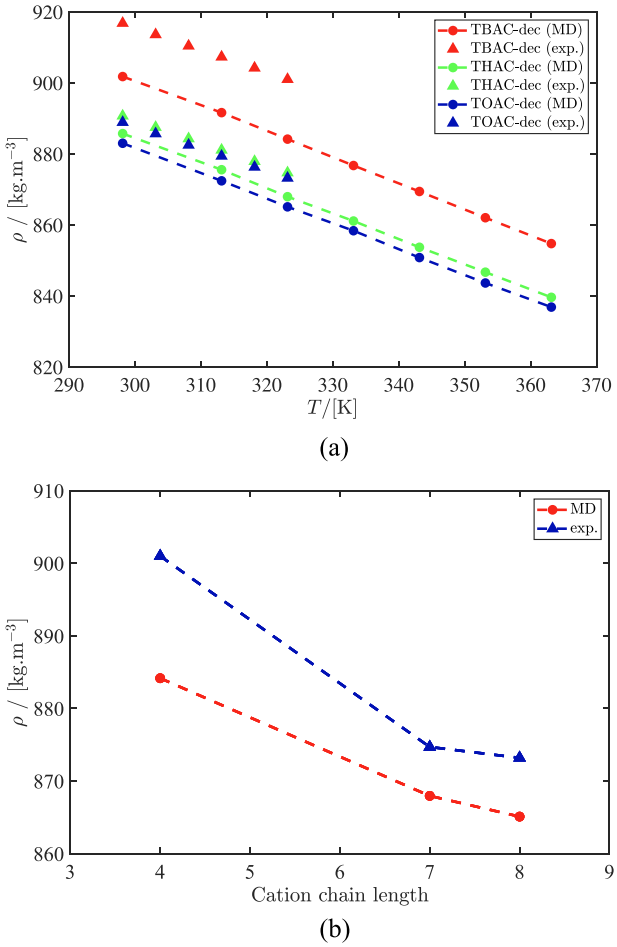

FIG. 3. Densities of TBAC-dec, THAC-dec, and TOAC-dec DESs (a) as a function of temperature and (b) as a function of cation alkyl chain length at 323.15 K, compared with experimental data by van Osch *et al.*[15] The dashed lines are added to guide the eye.

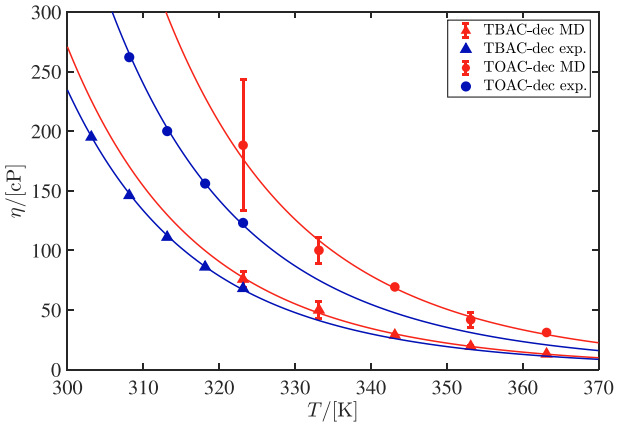

FIG. 4. Viscosities of TBAC-dec and TOAC-dec from MD simulations compared with experimental measurements by van Osch *et al.*[15] as a function of temperature. The solid curves denote the Arrhenius fitted curves. The errors bars that are smaller than the symbol size are not shown for clarity.

MD lie between those of TBAC-dec and TOAC-dec, although for clarity, the viscosity of THAC-dec is not depicted in Fig. 4. The computed viscosity data of all DESs from MD simulations are listed in Table S13 of the supplementary material. The viscosities of the DESs as a function of cation chain length are presented in Fig. S5 of the supplementary material, showing an increase with an increase in cation chain length at 343.15 K (observed at all temperatures). The increase in viscosity with the cation chain length may be associated with the additional dispersion forces of the chains, which promote friction with other molecules. Similarly, the experimental data of van Osch *et al.*[15] show an increase in the viscosity from TBAC-dec with a cation chain length of 4 to TOAC-dec with a cation chain length of 8. However, as mentioned in Sec. III A 1, the experimental viscosity of THAC-dec (with a chain length of 7) is reported lower than those of TBAC-dec and TOAC-dec, which may be due to a larger mole fraction-based water content of THAC-dec used in those experiments. The increase in viscosity with the cation chain length has also been observed for other DESs based on (tetra)alkylammonium halide HBAs.[100,101,105,106] Thus, to compare the computed viscosity of THAC-dec with experimental data, a "revised" set of experimental data (also shown in Fig. S5) was obtained for THAC-dec by interpolation from the experimental viscosities of TBAC-dec and TOAC-dec with respect to cation chain length. As mentioned previously, due to computational limitations, the viscosities were computed at $T \geq 323.15$ K. Therefore, the viscosities from MD simulations and experiments overlap in only one temperature point, i.e., at $T = 323.15$ K. However, the experimental viscosity data exhibit an Arrhenius temperature correlation ($R^2 = 0.9994$ for all DESs), which allowed for extrapolation to higher temperatures. It was observed that the computed viscosities with MD could also be fitted to an Arrhenius functional form with R^2 values of 0.9978, 0.9871, and 0.9916 for TBAC-dec, THAC-dec, and TOAC-dec, respectively, which may be used to predict viscosities at lower temperatures. The Arrhenius fitting curves for both simulation and experimental data are denoted by the solid curves in Fig. 4. As can be observed in Fig. 4, the computed viscosities agree reasonably well with the (extrapolated) experimental data of van Osch *et al.*[15] over a wide range of temperatures and cation chain lengths. The average relative deviations of the computed viscosities with respect to the extrapolated experimental data are 15%, 37%, and 44% for TBAC-dec, THAC-dec, and TOAC-dec, respectively. These findings indicate a systematic increase in the relative deviations from experimental data as the cation chain length increases, which is reasonable since the optimal force field parameters were chosen based on the density and viscosity of TBAC-dec. As mentioned previously, the DESs used in the experiments of van Osch *et al.*[15] contained some amounts of water (4640–8140 ppm), which may have lowered the measured viscosities. Moreover, the experimental viscosities reported by Ruggeri *et al.*[24] (429 cP) and Saydan *et al.*[84] (489 cP) for TBAC-dec at 298 K are larger than the ones reported by van Osch *et al.*[15] (265 cP), possibly due to

differences in the hydration level of the DES. Therefore, the viscosities of the anhydrous DESs are likely larger than those reported by van Osch *et al.*[15]

The relatively larger deviations of the simulated viscosities from the experimental data at larger cation chain lengths may be improved by further fine-tuning of the force field parameters for each DES, e.g., using smaller charge and/or LJ scaling factors at larger chain lengths. This would however compromise the transferability of the obtained force field parameters. Nevertheless, more experimental measurements are required for the viscosity of the DESs studied in this work (and hydrophobic DESs in general), without which it is difficult to provide accurate force field parameters. It should be noted that at larger cation chain lengths and lower temperatures (thus higher viscosities), the linear regime could not be achieved for the mean squared displacements (MSDs), which impeded the accurate calculation of viscosity values and resulted in larger uncertainties (as shown with error bars in Fig. 4). Furthermore, instead of averaging viscosities from the various independent runs, first, the MSDs of the independent runs were averaged, and subsequently, linear regression was performed on the averaged MSDs to obtain the average value of viscosity. This method enhanced the quality of the linear regression of the MSDs and is therefore recommended for the calculation of transport properties of viscous mixtures, such as DESs, using the Einstein formulation. As an example, the averaged MSDs (of the off-diagonal pressure tensor components) in TOAC-dec at 343.15 K are presented in Fig. S6 of the supplementary material, as a function of correlation time in a log–log plot. It is worth mentioning that often more complicated correlations such as the Vogel–Fulcher–Tammann (VFT) function are used to model the temperature dependence of viscosity of DESs.[8,81–83,107] The viscosity data in the present work could also be modeled well with the VFT function ($R^2 > 0.9989$ for all DESs), although the simple Arrhenius model showed sufficient capability for capturing the temperature dependence of viscosity for the studied DESs. The VFT model should be used with caution when extrapolating the viscosity data to lower temperatures, as it is known to overestimate viscosities at low temperatures.[108] Therefore, in the case of extrapolation to lower temperatures, other functional forms, e.g., Mauro–Yue–Ellison–Gupta–Allan (MYEGA) model, may be preferable.[108,109]

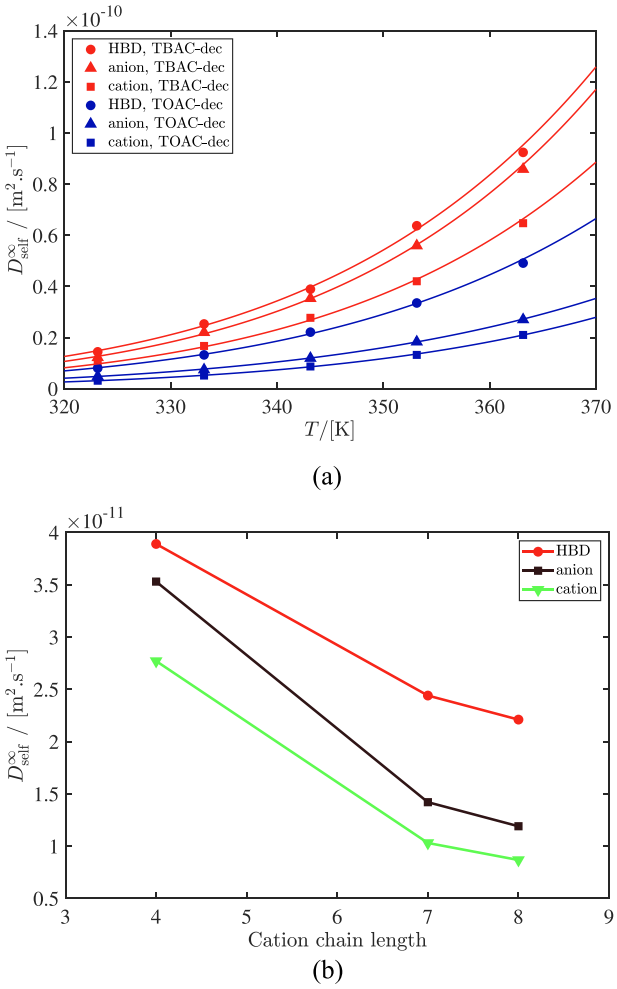

FIG. 5. Finite size-corrected self-diffusion coefficients for various DES components (a) as a function of temperature for TBAC-dec and TOAC-dec with the corresponding Arrhenius fitted curves (solid curves) and (b) as a function of cation alkyl chain length at 343.15 K. The lines in (b) are used to guide the eye.

4. Self-diffusivities

Self-diffusion coefficients were computed for HBD, cation, and anion components of the DESs at different temperatures based on the center-of-mass motion of the molecules. The resulting finite size-corrected diffusivities are presented in Fig. 5 as a function of temperature and as a function of cation chain length at 343.15 K. For clarity, the diffusivities of THAC-dec components are not shown in Fig. 5(a). The computed self-diffusion coefficient data for all DESs are listed in Tables S14–S16 of the supplementary material. It can be observed in Fig. 5 that for all DESs, the self-diffusion coefficients of all the components increase by increasing the temperature. All diffusivities obey an Arrhenius-type temperature dependence [shown by solid curves in Fig. 5(a)] with $R^2 > 0.998$. The Yeh–Hummer finite size corrections account for 10%–32% (on average 20%) of the final diffusion coefficients, as presented in Fig. 5. Unfortunately, no experimental data are available for diffusion coefficients of the DESs studied in this work, so a direct validation of the computed diffusivities is not possible.

As shown in Fig. 5, for all DESs and at all temperatures, the largest diffusion coefficient belongs to the HBD, while the cation exhibits the smallest diffusivity. A similar order for the diffusivity of DES components has been reported in the literature for several choline chloride-based DESs.[30,33,59,110] As can be observed in Fig. 5(b), the diffusion coefficients of all DES components decrease as the cation chain length is increased. This may be due to the stronger intermolecular interactions and thus higher viscosity of the DES mixtures with longer cation chains. Furthermore, with an increase in cation chain length, the hydrodynamic radius and molecular weight of the cation are increased. This may contribute to a further decrease in the mobility and self-diffusion coefficient of the cation. Figure 5(b) shows that as the cation alkyl chain length is

increased from 4 to 8, the difference between the diffusion coefficients of HBD and anion becomes larger, while the difference between the diffusion coefficients of anion and cation decreases. This effect was observed at all temperatures and may imply that at larger cation chain lengths, the motions of cations and anions are coupled, while this coupling is observed between the motions of HBDs and anions at smaller cation chain lengths. This is counterintuitive as one would expect an increase in cation chain length to reduce the anion–cation electrostatic interactions due to steric hindrance of the chains.

5. Ionic conductivities

Ionic conductivities of the DESs were calculated at various temperatures, based on the computed finite size-corrected diffusivities, and the results are presented in Fig. 6. The computed values for ionic conductivities of all DESs are also listed in Table S17 of the supplementary material. The ionic conductivities of all DESs become larger when the temperature is increased due to the enhanced diffusion of ions. Similar to viscosities and diffusivities, this temperature dependence could be described by an Arrhenius-type relationship (depicted by the solid curves in Fig. 6) with $R^2 > 0.9985$ for all DESs. As shown in Fig. 6, the ionic conductivity decreases with an increase in cation chain length at all temperatures, which is attributed to the slower diffusion of ions in DESs with longer cation chains. Comparable effects of cation chain length on the ionic conductivity have been observed for other DESs based on (tetraalkyl)ammonium halides.[100,111] Ruggeri *et al.*[24] reported an experimental ionic conductivity of ~40 μS cm^{-1} at 298 K for TBAC-dec with a water content of 0.11% (mass fraction-based). It is expected for the ionic conductivity of TBAC-dec with no water content to be even lower than 40 μS cm^{-1}, as the presence of water has been shown to increase the ionic conductivity of other DESs due to an increased mobility of ions.[33,112] When extrapolated to 298 K, the MD simulation results for TBAC-dec yield an ionic conductivity of 102 μS cm^{-1}. It is important to note that the Nernst–Einstein relation [Eq. (4)] neglects any cross correlation between the motions of different ions in the mixture.[76] Dong *et al.*[113] showed for aqueous solutions of tetraalkylammonium bromide IL, at various IL concentrations that ionic conductivities calculated from the Nernst–Einstein equation may be several times larger than the ones computed from the Einstein relation (using the cross correlation of charge displacements) due to a strongly correlated motion of the ions. Similarly, it is possible that for the DESs in the present work, the ionic conductivities are overestimated from Eq. (4) because of a strong correlation between the motions of cation and anion. It is also possible, however that this difference is simply caused by an overestimation of the diffusivities from the MD simulations. More experimental data are required for the transport properties of TRAC-dec DESs to provide more accurate conclusions in this regard.

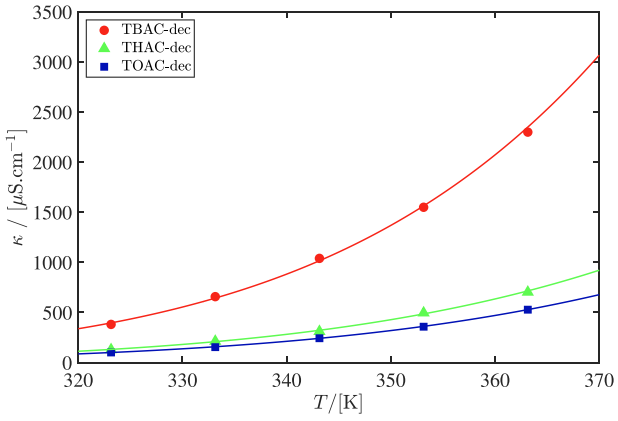

FIG. 6. Ionic conductivities of TBAC-dec, THAC-dec, and TOAC-dec as a function of temperature. The solid curves denote the corresponding Arrhenius fits.

B. Liquid structure

1. Radial distribution functions

To study the liquid structure of the DESs, partial RDFs were computed for different atom pairs in the mixtures. The RDFs for the most dominant interactions (largest peaks) are presented in Fig. 7 for TBAC-dec, THAC-dec, and TOAC-dec at 343.15 K. As shown in Fig. 7(a), for all DESs, a large RDF peak is observed at ~1.9 Å for the interaction between chloride (Cl) and the hydroxyl hydrogen of decanoic acid (HO), which implies a hydrogen bond between the two atoms. Strong hydrogen bonds between chloride anion and hydroxyl groups of HBDs or cations have also been reported for other (hydrophilic) DESs in the literature.[30,32,57,114] The RDFs for the interaction of the nitrogen atom of cation (N) with chloride show a peak (although smaller than that of the Cl–HO RDFs) at an average distance of ~4.3 Å, likely due to the cation–anion electrostatic interactions. As shown in Fig. 7(b), the RDFs for the interaction of the carbonyl oxygen (O) with the hydroxyl hydrogen of decanoic acid exhibit one large peak with a left shoulder, centered around 2.0 Å (the shoulder is at ~1.7 Å), and a smaller peak at 3.0 Å. By post-processing snapshots of atomic coordinates from the simulations, it was found that the left shoulder of the first peak corresponds to the intermolecular O–HO (hydrogen bond) interaction between different decanoic acid molecules, while the peaks at 2.0 and 3.0 Å correspond to O–HO intramolecular interactions in the same decanoic acid molecule. The decomposed O–HO RDF into intermolecular and intramolecular contributions is presented in Fig. S7 of the supplementary material for TBAC-dec at 343.15 K. By calculating the dihedral angle between the carbonyl oxygen and the hydroxyl hydrogen ($\phi_{\mathrm{O-HO}}$) of decanoic acid molecules, it was found that the peak positions of the O–HO intramolecular RDF represent two distinct dihedral angle ranges: The peak at 2.0 Å corresponds to $\phi_{\mathrm{O-HO}}$ values in the range of ~0° to 40° and thus a cis configuration between O and HO (on the same side of the molecule), whereas the peak at 3.0 Å corresponds to $\phi_{\mathrm{O-HO}}$ values in the range of ~140° to 180° and therefore a trans configuration (on opposite sides). This correlation between the dihedral angle and intramolecular O–HO distance is shown in Fig. S8 of the supplementary material. Based on the RDFs in Fig. 7(b), it may be concluded that the probability of finding the cis configuration between O and HO is larger than that of the trans configuration. The large intermolecular O–HO and Cl–HO peaks shown in Fig. 7 indicate that strong HBD–HBD and HBD–anion (hydrogen bond) interactions are present in all DESs. This is in contrast to the relatively weak HBD–cation interactions

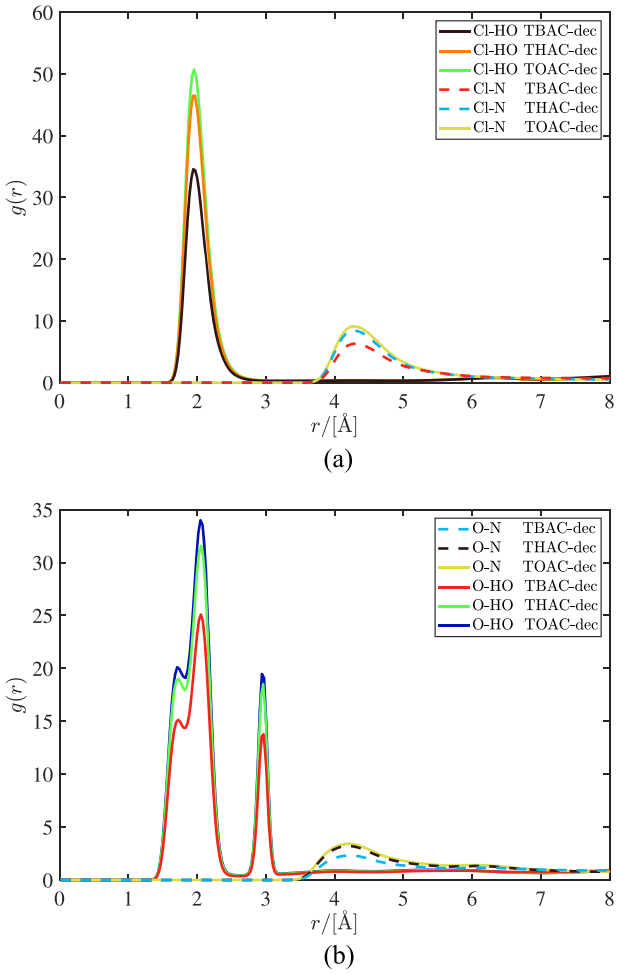

FIG. 7. RDFs for the interactions between (a) the chloride anion and hydroxyl hydrogen of decanoic acid (Cl–HO), and the chloride anion and the nitrogen atom of cation (Cl–N), and (b) the carbonyl oxygen of decanoic acid and the nitrogen atom of cation (O–N), and the carbonyl oxygen and hydroxyl hydrogen of decanoic acid (O–HO) from MD simulations of TBAC-dec, THAC-dec, and TOAC-dec hydrophobic DESs at 343.15 K.

as represented in Fig. 7(b) by the RDFs for the carbonyl oxygen of decanoic acid with respect to the nitrogen of cation (O–N). This may be due to the lack of hydrogen bond accepting/donating moieties on the cation, which prevents any considerable interaction with the HBD.

In the preliminary testing of the force field parameters for TBAC-dec at 298.15 K, it was found that by increasing the ionic charge scaling factor (approaching 1), the Cl–HO RDF peak intensity is significantly increased: from 33 at $f_q = 0.6$ up to 49 at $f_q = 0.7$ and 64 at $f_q = 0.8$ (shown in Fig. S9 of the supplementary material). Considering the negligible effect of the charge scaling on density (less than 0.5% at 298.15 K), such peak differences indicate the major contribution of electrostatic forces to the Cl–HO interaction. Furthermore, the Cl–HO peak position is slightly shifted to lower values at larger charge scaling factors, implying stronger electrostatic interactions. Perkins *et al.*[30] have reported a comparable influence of ionic charge scaling on the interaction between the hydroxyl group of the choline cation and chloride anion in choline chloride urea DESs. A similar, albeit less drastic, effect of the charge scaling is observed on the N–Cl RDF (Fig. S9). For the O–HO interaction, it was found that at larger charge scaling factors, the intensity of the intermolecular RDF peak decreases (Fig. S9). This is possibly due to a competition between the O–HO and Cl–HO (hydrogen bond) interactions, where larger ionic charge scaling factors and thus stronger Cl–HO (anion–HBD) interactions result in the weakening of O–HO interactions. Furthermore, at larger charge scaling factors, the intensity of the intramolecular O–HO peak at 2.0 Å decreases, while the intramolecular peak at 3.0 Å shows an increase in intensity (Fig. S9). This implies that by using larger charge scaling factors, the probability of the O–HO trans configuration increases, while the probability of the cis configuration is reduced. This may be caused by the stronger Cl–HO interactions at larger charge scaling factors: The HO atom is moved to the opposite side of the carbonyl oxygen to reduce the repulsive electrostatic interaction between chloride and carbonyl oxygen, both with relatively large negative (partial) charges.

As can be observed in Fig. 7(a), the intensities of the RDF peaks increase with increasing cation chain length. For instance, the Cl–HO RDFs show peak intensities of 35, 47, and 51 for TBAC-dec, THAC-dec, and TOAC-dec, respectively. This is mainly due to the difference in the simulation box volumes (and thus densities) of the DESs, with respect to which the RDFs are normalized, rather than profound differences in interactions and the heterogeneity of the DESs. Furthermore, the RDF peak positions are not influenced by the cation chain length. As shown in Fig. 7, the RDFs for the interactions of nitrogen (representing the center-of-mass of the cation) with other atoms exhibit the first peak at comparatively larger distances, which is consistent with RDFs reported for choline chloride urea.[33] This is likely due to the large size of the cation and the steric hindrance of its alkyl chains. It was found that all RDFs show negligible sensitivity to temperature with only a slight decrease in the peak intensities at higher temperatures (Fig. S10 of the supplementary material). This is consistent with other findings in the literature for DESs.[32,33] A more detailed presentation of the site–site RDFs for all DESs can be found in Figs. S11–S13 of the supplementary material. First solvation shell coordination numbers, calculated at 343.15 K from integration of the RDFs up to the first minimum, are also listed in Table S18 of the supplementary material. It is important to note that unlike RDFs, the coordination numbers do not depend on the system volume[75] and may therefore better reflect structural differences between systems of different densities. As shown in Table S18, the coordination numbers are not significantly affected by the cation chain length, confirming the negligible effect of the chain length on the liquid structure of the DESs. Only a slight decrease in the N–Cl coordination number is observed with longer cation chains, which is possibly due to the steric hindrance effects.

2. Hydrogen bonding

The results for the hydrogen bond analysis of the DESs are shown in Fig. 8 as a function of temperature for TBAC-dec and as

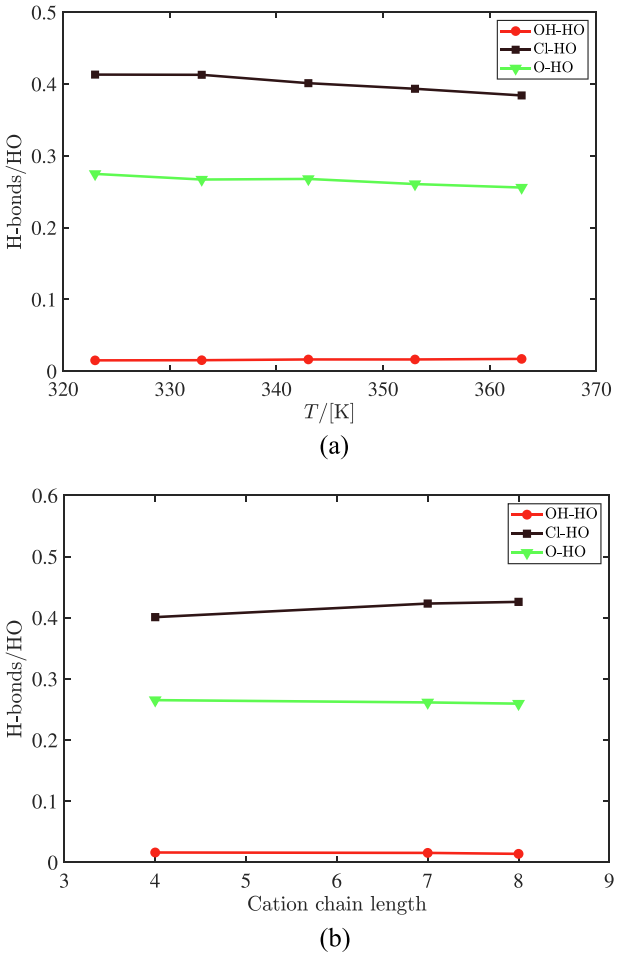

FIG. 8. Number of various types of hydrogen bonds per number of hydroxyl hydrogen atoms in the mixture as a function of (a) temperature for TBAC-dec and (b) cation chain length at 343.15 K. The solid lines are drawn to guide the eye.

a function of cation chain length at 343.15 K. The plots in Fig. 8 are presented in terms of the number of hydrogen bonds per number of hydroxyl hydrogen atoms in the system (H-bond/HO). For all DESs, 100 HO atoms (due to 100 decanoic acid molecules) were present in the system. Three types of hydrogen bonds were considered in the analysis: (1) between carbonyl oxygen and the hydroxyl hydrogen (O–HO) of decanoic acid, (2) between hydroxyl oxygen and hydroxyl hydrogen (OH–HO) of decanoic acid, and (3) between chloride and hydroxyl hydrogen (Cl–HO) of decanoic acid. As can be observed in Fig. 8, the Cl–HO hydrogen bond is found to be the most prominent type of hydrogen bond in TBAC-dec with ~0.4 H-bond/HO. To a lesser extent, O–HO hydrogen bonds are formed in the mixture with an average population of ~0.27 H-bond/HO, although this number includes both intermolecular and intramolecular interactions (as discussed for the RDFs). Only a small number of OH–HO hydrogen bonds (0.02 H-bond/HO) are found in the DESs, implying the preference of hydroxyl hydrogen of decanoic acid to the hydrogen bond to carbonyl oxygen, rather than hydroxyl oxygen, of other decanoic acid molecules. It is important to note that the strong HBD–HBD and HBD–anion hydrogen bonds may ultimately lead to proton transfers, which may affect the macroscopic properties of DESs. However, commonly used non-reactive atomic force fields, such as the GAFF force field used in this work, are not capable of modeling proton transfers. As depicted in Fig. 8(a), the number of hydrogen bonds does not change significantly as the temperature is increased. This temperature independence of the number of hydrogen bonds has also been reported by Celebi *et al.*[33] for MD simulations of choline chloride urea and choline chloride ethylene glycol DESs. As can be observed in Fig. 8(b), increasing the cation chain length does not have a considerable influence on the number of the various hydrogen bonds (only a slight increase in the number of Cl–HO hydrogen bonds). This is in agreement with the findings from the RDFs regarding the effect of cation chain length on the peak intensities and positions and the liquid structure. The insensitivity of the number of hydrogen bonds to the cation chain length was noticed at all temperatures (Fig. S14 of the supplementary material). Overall, based on the results from the RDFs and the hydrogen bond analysis, the liquid structures of the DESs with various cation chain lengths are almost identical, and the same intermolecular interactions dominate all the mixtures. This is in sharp contrast to the transport properties (and to a lesser degree the density) of these DESs, which are found to be considerably affected by the cation chain length. It is therefore postulated that such differences in density and transport properties are caused mainly by the larger size of the cation, affecting the packing of molecules and resulting in stronger frictional forces (due to the dispersion forces of the chains), rather than extensive structural changes in the liquid mixture. It would be interesting for a future work to systematically examine, at the nanoscale, how the transport and structural properties of these DESs alter with the chain length of the HBD component.

IV. CONCLUSIONS

MD simulations were performed to compute the densities, transport, and structural properties of tetraalkylammonium chloride decanoic acid DESs with cation chain lengths of 4, 7, and 8. A modified GAFF force field with an ionic charge scaling factor of 0.6 was used to model all DESs. The computed densities and viscosities of the DESs were in reasonable agreement with experimental data found in the literature. An increase in the cation chain length was observed to decrease the density of the DESs, possibly due to a hindered packing of molecules. The viscosity of the DESs increased with increasing cation chain length, suggesting stronger intermolecular interactions and larger molecular friction. Consistently, the self-diffusion coefficients and ionic conductivity decreased when the cation chain length was increased due to a lower mobility of molecules/ions. The self-diffusion coefficients of the various components exhibited the following order in all DES systems: HBD > anion > cation. The computed RDFs showed significant (hydrogen bond) interactions between the hydroxyl and the carbonyl groups of decanoic acid as well as between the hydroxyl group

of decanoic acid and chloride anions. The hydrogen bond analysis corroborated the results from the RDFs, while also indicating a negligible number of hydroxyl–hydroxyl hydrogen bonds between decanoic acid molecules. The effect of cation chain length on the RDFs and hydrogen bond populations was observed to be insignificant, in sharp contrast to its pronounced influence on the transport properties.

SUPPLEMENTARY MATERIAL

See the supplementary material for molecular structure and force field parameters of the studied DESs and additional MD simulation results.

ACKNOWLEDGMENTS

This work was sponsored by NWO Exacte Wetenschappen (Physical Sciences) for the use of supercomputer facilities with financial support from the Nederlandse Organisatie voor Wetenschappelijk Onderzoek (The Netherlands Organisation for Scientific Research, NWO). T.J.H.V. acknowledges NWO-CW (Chemical Sciences) for a VICI grant.

DATA AVAILABILITY

The data that support the findings of this study are available within the article and its supplementary material.

REFERENCES

[1]A. P. Abbott, G. Capper, D. L. Davies, R. K. Rasheed, and V. Tambyrajah, Chem. Commun. **2003**, 70.
[2]Q. Zhang, K. De Oliveira Vigier, S. Royer, and F. Jérôme, Chem. Soc. Rev. **41**, 7108 (2012).
[3]Y. Marcus, *Deep Eutectic Solvents* (Springer International Publishing, Cham, Switzerland, 2019), Vol. 1.
[4]E. L. Smith, A. P. Abbott, and K. S. Ryder, Chem. Rev. **114**, 11060 (2014).
[5]S. Sarmad, Y. Xie, J. P. Mikkola, and X. Ji, New J. Chem. **41**, 290 (2016).
[6]D. J. G. P. van Osch, C. H. J. T. Dietz, S. E. E. Warrag, and M. C. Kroon, ACS Sustainable Chem. Eng. **8**, 10591 (2020).
[7]A. Paiva, R. Craveiro, I. Aroso, M. Martins, R. L. Reis, and A. R. C. Duarte, ACS Sustainable Chem. Eng. **2**, 1063 (2014).
[8]B. B. Hansen, S. Spittle, B. Chen, D. Poe, Y. Zhang, J. M. Klein, A. Horton, L. Adhikari, T. Zelovich, B. W. Doherty, B. Gurkan, E. J. Maginn, A. Ragauskas, M. Dadmun, T. A. Zawodzinski, G. A. Baker, M. E. Tuckerman, R. F. Savinell, and J. R. Sangoro, Chem. Rev. **121**, 1232 (2021).
[9]G. García, S. Aparicio, R. Ullah, and M. Atilhan, Energy Fuels **29**, 2616 (2015).
[10]M. A. R. Martins, S. P. Pinho, and J. A. P. Coutinho, J. Solution Chem. **48**, 962 (2019).
[11]Y. Liu, J. B. Friesen, J. B. McAlpine, D. C. Lankin, S.-N. Chen, and G. F. Pauli, J. Nat. Prod. **81**, 679 (2018).
[12]D. O. Abranches, M. A. R. Martins, L. P. Silva, N. Schaeffer, S. P. Pinho, and J. A. P. Coutinho, Chem. Commun. **55**, 10253 (2019).
[13]L. J. B. M. Kollau, M. Vis, A. van den Bruinhorst, A. C. C. Esteves, and R. Tuinier, Chem. Commun. **54**, 13351 (2018).
[14]C. Florindo, L. C. Branco, and I. M. Marrucho, ChemSusChem **12**, 1549 (2019).
[15]D. J. G. P. van Osch, L. F. Zubeir, A. van den Bruinhorst, M. A. A. Rocha, and M. C. Kroon, Green Chem. **17**, 4518 (2015).
[16]L. F. Zubeir, D. J. G. P. van Osch, M. A. A. Rocha, F. Banat, and M. C. Kroon, J. Chem. Eng. Data **63**, 913 (2018).
[17]C. H. J. T. Dietz, D. J. G. P. van Osch, M. C. Kroon, G. Sadowski, M. van Sint Annaland, F. Gallucci, L. F. Zubeir, and C. Held, Fluid Phase Equilib. **448**, 94 (2017).
[18]M. B. Haider, D. Jha, R. Kumar, and B. Marriyappan Sivagnanam, Int. J. Greenhouse Gas Control **92**, 102839 (2020).
[19]W. Tang, Y. Dai, and K. H. Row, Anal. Bioanal. Chem. **410**, 7325 (2018).
[20]C. H. J. T. Dietz, M. C. Kroon, M. van Sint Annaland, and F. Gallucci, J. Chem. Eng. Data **62**, 3633 (2017).
[21]C. H. J. T. Dietz, A. Erve, M. C. Kroon, M. van Sint Annaland, F. Gallucci, and C. Held, Fluid Phase Equilib. **489**, 75 (2019).
[22]E. E. Tereshatov, M. Y. Boltoeva, and C. M. Folden, Green Chem. **18**, 4616 (2016).
[23]T. E. Phelps, N. Bhawawet, S. S. Jurisson, and G. A. Baker, ACS Sustainable Chem. Eng. **6**, 13656 (2018).
[24]S. Ruggeri, F. Poletti, C. Zanardi, L. Pigani, B. Zanfrognini, E. Corsi, N. Dossi, M. Salomäki, H. Kivelä, J. Lukkari, and F. Terzi, Electrochim. Acta **295**, 124 (2019).
[25]S. Zhu, J. Zhou, H. Jia, and H. Zhang, Food Chem. **243**, 351 (2018).
[26]R. Verma and T. Banerjee, Ind. Eng. Chem. Res. **57**, 3371 (2018).
[27]J. P. Wojeicchowski, A. M. Ferreira, D. O. Abranches, M. R. Mafra, and J. A. P. Coutinho, ACS Sustainable Chem. Eng. **8**, 12132 (2020).
[28]I. Adeyemi, R. Sulaiman, M. Almazroui, A. Al-Hammadi, and I. M. AlNashef, J. Mol. Liq. **311**, 113180 (2020).
[29]D. Rodríguez-Llorente, A. Cañada-Barcala, C. Muñoz, G. Pascual-Muñoz, P. Navarro, R. Santiago, V. I. Águeda, S. Álvarez-Torrellas, J. García, and M. Larriba, Sep. Purif. Technol. **251**, 117379 (2020).
[30]S. L. Perkins, P. Painter, and C. M. Colina, J. Phys. Chem. B **117**, 10250 (2013).
[31]S. L. Perkins, P. Painter, and C. M. Colina, J. Chem. Eng. Data **59**, 3652 (2014).
[32]E. S. C. Ferreira, I. V. Voroshylova, C. M. Pereira, and M. N. D. S. Cordeiro, J. Phys. Chem. B **120**, 10124 (2016).
[33]A. T. Celebi, T. J. H. Vlugt, and O. A. Moultos, J. Phys. Chem. B **123**, 11014 (2019).
[34]B. Doherty and O. Acevedo, J. Phys. Chem. B **122**, 9982 (2018).
[35]D. Shah and F. S. Mjalli, Phys. Chem. Chem. Phys. **16**, 23900 (2014).
[36]S. Mainberger, M. Kindlein, F. Bezold, E. Elts, M. Minceva, and H. Briesen, Mol. Phys. **115**, 1309 (2017).
[37]H. S. Salehi, M. Ramdin, O. A. Moultos, and T. J. H. Vlugt, Fluid Phase Equilib. **497**, 10 (2019).
[38]S. Kaur, A. Gupta, and H. K. Kashyap, J. Phys. Chem. B **120**, 6712 (2016).
[39]J. Baz, C. Held, J. Pleiss, and N. Hansen, Phys. Chem. Chem. Phys. **21**, 6467 (2019).
[40]G. García, M. Atilhan, and S. Aparicio, J. Phys. Chem. C **119**, 21413 (2015).
[41]H. S. Salehi, R. Hens, O. A. Moultos, and T. J. H. Vlugt, J. Mol. Liq. **316**, 113729 (2020).
[42]T. Zhekenov, N. Toksanbayev, Z. Kazakbayeva, D. Shah, and F. S. Mjalli, Fluid Phase Equilib. **441**, 43 (2017).
[43]R. Verma, M. Mohan, V. V. Goud, and T. Banerjee, ACS Sustainable Chem. Eng. **6**, 16920 (2018).
[44]N. Paul, P. K. Naik, B. D. Ribeiro, P. S. Gooh Pattader, I. M. Marrucho, and T. Banerjee, J. Phys. Chem. B **124**, 7405 (2020).
[45]D. Frenkel and B. Smit, *Understanding Molecular Simulation: From Algorithms to Applications*, 2nd ed. (Academic Press, San Diego, CA, 2002), Vol. 1.
[46]M. P. Allen and D. J. Tildesley, *Computer Simulation of Liquids*, 2nd ed. (Oxford University Press, Inc., New York, NY, 2017).
[47]P. V. A. Pontes, E. A. Crespo, M. A. R. Martins, L. P. Silva, C. M. S. S. Neves, G. J. Maximo, M. D. Hubinger, E. A. C. Batista, S. P. Pinho, J. A. P. Coutinho, G. Sadowski, and C. Held, Fluid Phase Equilib. **448**, 69 (2017).
[48]Y. Zhang and E. J. Maginn, Phys. Chem. Chem. Phys. **16**, 13489 (2014).
[49]J. Wang, R. M. Wolf, J. W. Caldwell, P. A. Kollman, and D. A. Case, J. Comput. Chem. **25**, 1157 (2004).
[50]T. Fox and P. A. Kollman, J. Phys. Chem. B **102**, 8070 (1998).

[51] C. I. Bayly, P. Cieplak, W. Cornell, and P. A. Kollman, J. Phys. Chem. **97**, 10269 (1993).
[52] M. J. Frisch, G. W. Trucks, H. B. Schlegel, G. E. Scuseria, M. A. Robb, J. R. Cheeseman, G. Scalmani, V. Barone, B. Mennucci, G. A. Petersson, H. Nakatsuji, M. Caricato, X. Li, H. P. Hratchian, A. F. Izmaylov, J. Bloino, G. Zheng, J. L. Sonnenberg, M. Hada, M. Ehara, K. Toyota, R. Fukuda, J. Hasegawa, M. Ishida, T. Nakajima, Y. Honda, K. Kitao, H. Nakai, T. Vreven, J. A. Montgomery, Jr., J. E. Peralta, F. Ogliaro, M. Bearpark, J. J. Heyd, E. Brothers, K. N. Kudin, V. N. Staroverov, T. Keith, R. Kobayashi, J. Normand, K. Raghavachari, A. Rendell, J. C. Burant, S. S. Iyengar, J. Tomasi, M. Cossi, N. Rega, J. M. Millam, M. Klene, J. E. Knox, J. B. Cross, V. Bakken, C. Adamo, J. Jaramillo, R. Gomperts, R. E. Stratmann, O. Yazyev, A. J. Austin, R. Cammi, C. Pomelli, J. W. Ochterski, R. L. Martin, K. Morokuma, V. G. Zakrzewski, G. A. Voth, P. Salvador, J. J. Dannenberg, S. Dapprich, A. D. Daniels, O. Farkas, J. B. Foresman, J. V. Ortiz, J. Cioslowski, and D. J. Fox, *Gaussian 09*, Revision B.01, Gaussian, Inc., Wallingford, CT, 2010.
[53] F.-Y. Dupradeau, A. Pigache, T. Zaffran, C. Savineau, R. Lelong, N. Grivel, D. Lelong, W. Rosanski, and P. Cieplak, Phys. Chem. Chem. Phys. **12**, 7821 (2010).
[54] A. González de Castilla, J. P. Bittner, S. Müller, S. Jakobtorweihen, and I. Smirnova, J. Chem. Eng. Data **65**, 943 (2020).
[55] V. Chaban, Phys. Chem. Chem. Phys. **13**, 16055 (2011).
[56] H. Liu and E. Maginn, J. Chem. Phys. **135**, 124507 (2011).
[57] B. Doherty, X. Zhong, S. Gathiaka, B. Li, and O. Acevedo, J. Chem. Theory Comput. **13**, 6131 (2017).
[58] T. Köddermann, D. Paschek, and R. Ludwig, ChemPhysChem **8**, 2464 (2007).
[59] A. Chaumont, E. Engler, and R. Schurhammer, J. Phys. Chem. B **124**, 7239 (2020).
[60] S. H. Jamali, T. V. Westen, O. A. Moultos, and T. J. H. Vlugt, J. Chem. Theory Comput. **14**, 6690 (2018).
[61] C. I. Bayly, K. M. Merz, D. M. Ferguson, W. D. Cornell, T. Fox, J. W. Caldwell, P. A. Kollman, P. Cieplak, I. R. Gould, and D. C. Spellmeyer, J. Am. Chem. Soc. **117**, 5179 (1995).
[62] L. Verlet, Phys. Rev. **159**, 98 (1967).
[63] L. Martínez, R. Andrade, E. G. Birgin, and J. M. Martínez, J. Comput. Chem. **30**, 2157 (2009).
[64] S. Plimpton, J. Comput. Phys. **117**, 1 (1995).
[65] W. Humphrey, A. Dalke, and K. Schulten, J. Mol. Graphics **14**, 33 (1996).
[66] S. H. Jamali, L. Wolff, T. M. Becker, M. de Groen, M. Ramdin, R. Hartkamp, A. Bardow, T. J. H. Vlugt, and O. A. Moultos, J. Chem. Inf. Model. **59**, 1290 (2019).
[67] P. Ganguly and N. F. A. van der Vegt, J. Chem. Theory Comput. **9**, 1347 (2013).
[68] J. Milzetti, D. Nayar, and N. F. A. van der Vegt, J. Phys. Chem. B **122**, 5515 (2018).
[69] D. Dubbeldam, D. C. Ford, D. E. Ellis, and R. Q. Snurr, Mol. Simul. **35**, 1084 (2009).
[70] A. T. Celebi, S. H. Jamali, A. Bardow, T. J. H. Vlugt, and O. A. Moultos, "Finite-size effects of diffusion coefficients computed from molecular dynamics: A review of what we have learned so far," Mol. Simul. (published online).
[71] S. H. Jamali, R. Hartkamp, C. Bardas, J. Söhl, T. J. H. Vlugt, and O. A. Moultos, J. Chem. Theory Comput. **14**, 5959 (2018).
[72] O. A. Moultos, Y. Zhang, I. N. Tsimpanogiannis, I. G. Economou, and E. J. Maginn, J. Chem. Phys. **145**, 074109 (2016).
[73] I.-C. Yeh and G. Hummer, J. Phys. Chem. B **108**, 15873 (2004).
[74] S. H. Jamali, A. Bardow, T. J. H. Vlugt, and O. A. Moultos, J. Chem. Theory Comput. **16**, 3799 (2020).
[75] M. T. Humbert, Y. Zhang, and E. J. Maginn, J. Chem. Inf. Model. **59**, 1301 (2019).
[76] K.-M. Tu, R. Ishizuka, and N. Matubayasi, J. Chem. Phys. **141**, 044126 (2014).
[77] M.-P. Florian, Acta Polym. **45**, 259 (1994).
[78] A. Luzar and D. Chandler, Phys. Rev. Lett. **76**, 928 (1996).
[79] W. Zhao, F. Leroy, B. Heggen, S. Zahn, B. Kirchner, S. Balasubramanian, and F. Müller-Plathe, J. Am. Chem. Soc. **131**, 15825 (2009).
[80] M. Kohagen, M. Brehm, Y. Lingscheid, R. Giernoth, J. Sangoro, F. Kremer, S. Naumov, C. Iacob, J. Kärger, R. Valiullin, and B. Kirchner, J. Phys. Chem. B **115**, 15280 (2011).
[81] A. Yadav and S. Pandey, J. Chem. Eng. Data **59**, 2221 (2014).
[82] A. Yadav, S. Trivedi, R. Rai, and S. Pandey, Fluid Phase Equilib. **367**, 135 (2014).
[83] K. R. Siongco, R. B. Leron, and M.-H. Li, J. Chem. Thermodyn. **65**, 65 (2013).
[84] G. Saydan, E. Yilmaz, and M. Soylak, J. Mol. Liq. **279**, 571 (2019).
[85] B. L. Bhargava and S. Balasubramanian, J. Chem. Phys. **127**, 114510 (2007).
[86] C. Schröder, Phys. Chem. Chem. Phys. **14**, 3089 (2012).
[87] N. Vergadou, E. Androulaki, J.-R. Hill, and I. G. Economou, Phys. Chem. Chem. Phys. **18**, 6850 (2016).
[88] T. G. A. Youngs and C. Hardacre, ChemPhysChem **9**, 1548 (2008).
[89] D. Shah, D. Gapeyenko, A. Urakpayev, and M. Torkmahalleh, J. Mol. Liq. **274**, 254 (2019).
[90] I. Leontyev and A. Stuchebrukhov, Phys. Chem. Chem. Phys. **13**, 2613 (2011).
[91] K. Wendler, F. Dommert, Y. Y. Zhao, R. Berger, C. Holm, and L. Delle Site, Faraday Discuss. **154**, 111 (2012).
[92] C. Florindo, A. J. McIntosh, T. Welton, L. C. Branco, and I. M. Marrucho, Phys. Chem. Chem. Phys. **20**, 206 (2017).
[93] A. R. R. Teles, E. V. Capela, R. S. Carmo, J. A. P. Coutinho, A. J. D. Silvestre, and M. G. Freire, Fluid Phase Equilib. **448**, 15 (2017).
[94] A. Pandey and S. Pandey, J. Phys. Chem. B **118**, 14652 (2014).
[95] D. Dubbeldam, S. Calero, and T. J. H. Vlugt, Mol. Simul. **44**, 653 (2018).
[96] T. L. Greaves, A. Weerawardena, C. Fong, I. Krodkiewska, and C. J. Drummond, J. Phys. Chem. B **110**, 22479 (2006).
[97] M. H. Ghatee, M. Zare, F. Moosavi, and A. R. Zolghadr, J. Chem. Eng. Data **55**, 3084 (2010).
[98] S. B. Capelo, T. Méndez-Morales, J. Carrete, E. López Lago, J. Vila, O. Cabeza, J. R. Rodríguez, M. Turmine, and L. M. Varela, J. Phys. Chem. B **116**, 11302 (2012).
[99] A. Filippov, M. Taher, F. U. Shah, S. Glavatskih, and O. N. Antzutkin, Phys. Chem. Chem. Phys. **16**, 26798 (2014).
[100] Z. Chen, M. Ludwig, G. G. Warr, and R. Atkin, J. Colloid Interface Sci. **494**, 373 (2017).
[101] B. Nowosielski, M. Jamrógiewicz, J. Łuczak, M. Śmiechowski, and D. Warmińska, J. Mol. Liq. **309**, 113110 (2020).
[102] D. Deng, Y. Jiang, X. Liu, Z. Zhang, and N. Ai, J. Chem. Thermodyn. **103**, 212 (2016).
[103] L. F. Zubeir, C. Held, G. Sadowski, and M. C. Kroon, J. Phys. Chem. B **120**, 2300 (2016).
[104] L. T. Eremenko, Bull. Acad. Sci. USSR, Div. Chem. Sci. **17**, 1012 (1968).
[105] L. F. Zubeir, M. H. M. Lacroix, and M. C. Kroon, J. Phys. Chem. B **118**, 14429 (2014).
[106] S. S. Hossain, S. Paul, and A. Samanta, J. Phys. Chem. B **123**, 6842 (2019).
[107] A. R. Harifi-Mood and R. Buchner, J. Mol. Liq. **225**, 689 (2017).
[108] Q. Zheng and J. C. Mauro, J. Am. Ceram. Soc. **100**, 6 (2017).
[109] A. F. Bouarab, J.-P. Harvey, and C. Robelin, Phys. Chem. Chem. Phys. **23**, 733 (2021).
[110] C. D'Agostino, R. C. Harris, A. P. Abbott, L. F. Gladden, and M. D. Mantle, Phys. Chem. Chem. Phys. **13**, 21383 (2011).
[111] G. Li, Y. Jiang, X. Liu, and D. Deng, J. Mol. Liq. **222**, 201 (2016).
[112] V. Agieienko and R. Buchner, J. Chem. Eng. Data **64**, 4763 (2019).
[113] D. Dong, J. B. Hooper, and D. Bedrov, J. Phys. Chem. B **121**, 4853 (2017).
[114] O. S. Hammond, D. T. Bowron, and K. J. Edler, Green Chem. **18**, 2736 (2016).